Detection of Gravity Modes in RR Lyrae Stars

Merieme Chadid

CrossMark

Detection of Gravity Modes in RR Lyrae Stars

Merieme Chadid
University of Côte d'Azur, Nice Sophia-Antipolis University, CNRS-UMR 7250, CS 34229, F-06304 NICE Cedex 4, France; chadid@unice.fr
Received 2021 June 23; revised 2021 November 4; accepted 2021 November 4; published 2022 January 31

Abstract

We report the detection of gravity modes in RR Lyrae stars. Thanks to Photometer AntarctIca eXtinction (PAIX), the first Antarctic polar photometer. Unprecedented and uninterrupted *UBVRI* time-series photometric ground-based data are collected during 150 days from the highest plateau of Antarctica. PAIX light-curve analyses reveal an even richer power spectrum with mixed modes in RR Lyrae stars. The nonlinear nature of several dominant peaks, showing lower and higher frequencies, occurs around the dominant fundamental radial pressure mode. These lower frequencies and harmonics linearly interact with the dominant fundamental radial pressure mode and its second and third overtone pressure modes, as well. Half-integer frequencies are also detected, likewise side-peak structures, demonstrating that HH Puppis is a bona-fide Blazhko star. Fourier correlations are used to derive underlying physical characteristics for HH Puppis. The most striking finding is the direct detection of gravity waves. We interpret the excitation mechanism of gravity waves in RR Lyrae stars by the penetrative convection-driving mechanism. We demonstrate that RR Lyrae stars' pulsation is excited by several distinct mechanisms, and hence RR Lyrae stars are simultaneously *g*-mode and *p*-mode pulsators. Our discoveries make RR Lyrae stars very challenging stellar objects, and provide their potential to undergo at the same time *g* and *p* modes toward an advancement of the theory of stellar evolution and a better understanding of the universe.

Unified Astronomy Thesaurus concepts: Observational astronomy (1145); Photometer (2030); Astronomy data analysis (1858); Pulsating variable stars (1307); Stellar convection envelopes (299); Stellar pulsations (1625); RR Lyrae variable stars (1410); Metallicity (1031); Chemical abundances (224)

Supporting material: machine-readable table

1. Introduction

Stellar pulsation and asteroseismology, the real music of the spheres, are a good clue toward an understanding of the internal structure and dynamics of stars from oscillations observed at their surfaces. Different modes penetrate to different depths in the star. Mathematically, there are two main sets of solutions to the equation of motion for an oscillating star, leading to two types of pulsation modes. In the *p* modes, acoustic waves, pressure is the primary restoring force for a star perturbed from equilibrium. The *p* modes are most sensitive to conditions in the outer part of the star. In the *g* modes, gravity waves, buoyancy is the restoring force. They are most sensitive to conditions in the deep interior of the star. In principle, the *g* modes have a finite amplitude in the outer part of star and are observed on the surface, as well. Otherwise, in massive main-sequence stars, the *g* mode is confined outside the convective core. For years, a major research topic was taken up with the big challenge in finding the *g* modes and providing a possible mechanism of their excitation.

RR Lyrae stars are considered to be classical radial pulsators, oscillating in *p* modes. Most of them are monoperiodic stars with an oscillation period near half a day. They are of enormous cosmological and galactic importance. Extreme Population II RR Lyrae stars were discovered first in globular clusters by Bailey in 1895. They are low-mass stars and are used to estimate the distance and the age of the clusters. Known as standard candles of galactic evolution, RR Lyrae stars have been observed for more than a century and subdivided into two Bailey classes, RRab and RRc stars (Bailey 1902). Such classification is based on the skewness and amplitude of the light curve, and the pulsation period, as well. A fourth class, RR d, was introduced later, oscillating in both the fundamental and first overtone. Spectroscopy studies have demonstrated that RR Lyrae stars are affected by nonradial oscillations, as well (Chadid et al. 1999). Such stars are also affected by hypersonic shock waves (Chadid et al. 2008).

However, the big challenge is the Blazhko effect (Blažko 1907). More than a century after its discovery, the Blazhko effect still remains a mystery. This greatly complicates the accurate measurement of the atmospheric dynamics of RR Lyrae stars and introduces unavoidable complications in an understanding of stellar pulsation and evolution. The most popular model trying to explain the Blazhko effect predicts the dependence of the Blazhko amplitude upon the strength of a magnetic field of the order of 1.5 kG, the oblique–dipole rotator model (Shibahashi & Takata 1995). Having covered several pulsation periods and Blazhko cycles spread over a period of 4 yr with high-precision longitudinal magnetic field measurements, Chadid et al. (2004) reported no detection of magnetic fields in RR Lyrae stars, and concluded that no magnetic model is able to explain the Blazhko effect, and so further understanding of the origin of the Blazhko effect still required new observations. Recently, Stothers (2010) has proposed a new explanation of the Blazhko effect caused by changes in the structure of the outer convective zone, generated by an irregular variation of the magnetic field. A resonance between a radial mode and a nonradial mode hypothesis (Nowakowski & Dziembowski 2001; Dziembowski & Mizerski 2004), and a

radial-mode resonance hypothesis (Buchler & Kolláth 2011) were also suggested to explain the Blazhko effect.

Up to now, the best applications in the study of RR Lyrae stars have relied dominantly on classical ground-based data sets (Alcock et al. 2003 and Soszyński et al. 2019), improved progressively by use of space telescopes such as CoRoT (Auvergne et al. 2009; Chadid 2012), Kepler (Gilliland et al. 2010; Benkő et al. 2014; Molnár et al. 2015), and TESS (Molnár et al. 2022), and lately accomplished by implementing a new way, Antarctic polar observations with Photometer AntarctIca eXtinction (PAIX): long, uninterrupted, and continuous precision observations over 150 days from the ground, one polar night, and without the regular interruptions imposed by the Earth's rotation (Chadid & Vernin 2019; Chadid et al. 2014).

The paper is organized as follows. In Section 2 we briefly describe the observations and the data-reduction process. The description and application of the methods used for the frequency analysis are presented in Section 3. The fundamental parameters, shock waves, and dynamics are discussed in Sections 4 and 5. In Section 6, we demonstrate the g-mode detection and we provide an explanation. Finally, some concluding remarks and our future plans are given in Section 7.

2. Observations and Data Reduction

2.1. PAIX (First Robotic Antarctic Photometer)

PAIX, the first robotic multiband photometer (Chadid et al. 2018), has been weatherproofed and robotized to run under extreme weather and human conditions, with temperatures as low as $-83°$C and altitude higher than 4000 m according to the low pressure at latitude $= -75°$ in the heart of Antarctica. PAIX is attached to the Cassegrain focus of a 40 cm Ritchey–Chretien optical telescope, with a F/D ratio of 10, supported by an equatorial-mount AstroPhysics 1200, and operates in the open field without any shelter. At the focus have been successively installed a robot-focus (Optec TCF), a filter wheel (SBIG-CFW6) equipped with Johnson–Cousins filters, and a CCD dual chip (SBIG-ST10-XME), all included in a thermalized box. These installations collect simultaneously the multicolor light curves of several targets within the same $12'.2 \times 8'.2$ field of view. All PAIX components are remotely controlled and set up through PAIX ACquisition Software (PACS) implemented on the PAIX experiment in Antarctica, accessible from anywhere through a virtual private network and a remote desktop. For more technical details on the PAIX multiband photometer and data, we refer to the invited SPIE paper (Chadid et al. 2016).

2.2. PAIX Observations

The PAIX data used in this study are the calibrated light curves from the magnitude extraction that we measured by PAIX's CCD during an observing run starting on 2011 May 12 and ending on 2011 September 25. The 17,500 CCD images of the target, HH Puppis, 11.31 V_{mag}, with J2000 α R.A. (right ascension)$07^h20^m35^s55$ and δ decl. (declination)$- 46^h42^m30^s11$, have been collected through UBVRI color filters with an exposure time $\Delta t \leqslant 60$ s, and processed even when the Sun was at $8°$ below horizon. In this case, the accumulated observable time spans, without any interruption, over 136 days of 2011's polar wintertime. We use for our purpose the V-filter passband in the Bessel Johnson–Cousins system (Bessell 2005), which stands for

an effective wavelength midpoint $\lambda_{eff} = 540$ nm and FWHM $\Delta\lambda = 100$ nm. Such spectral bandpass is 4.5 times narrower than the Kepler bandpass, which is from 400 to 850 nm (Koch et al. 2010).

2.3. PAIX Data Processing Pipeline (PPP)

The PAIX Pipeline Package (PPP) provides workflows for processing PAIX-observed polar photometric data. Such a software tool has been developed and maintained to provide measurements of both magnitude and extinction extractions and their precision toward light curves and Bouguer's lines simultaneously (Chadid & Vernin 2019). The PPP is principally based on a set of four softwares: (1) raw UBVRI images are corrected from dark, bias, flat fields and then corrected for hot pixels; the measurements of the magnitude of each star is performed with use of Sextractor; (2) the coordinates of the target and the position of a given known reference star are determined with the target magnitude precision; (3) the previous processing is used to plot light curves; and, finally, (4) the magnitude variation of the reference star as a function of the air mass is analyzed to compute the extinction coefficient, according to Bouguer's theory, and plots Bouguer's lines.

3. Detection of Frequencies and Results

Figure 1 shows the PAIX HH Puppis light curve folded with the pulsation period 0.390 day over 136 days. The PAIX data of HH Puppis provide 349 consecutive pulsation cycles and an homogeneous and uninterrupted coverage.

A frequency analysis of the photometric data was performed using Period04 (Lenz & Breger 2005) and PDM (Zalian et al. 2014). Both softwares perform a projection of the discrete photometric signal on a trigonometric basis and all led to the same results, with a slight difference at higher orders. In this study, we present the results of the Period04 frequency analysis. The Fourier decomposition consists of fitting the magnitude measurements by means of the series

$$m(t) = A_0 + \sum_{i=1,N} A_i \sin[2\pi(F_i(t - T_0) + \Phi_i)], \qquad (1)$$

where T_0 is the initial epoch value of the data set PAIXJD $T_0 = 245,569$, and Φ the normalized phase.

3.1. Fundamental Radial Pressure Mode and Harmonics

The original spectrum is dominated by the main pulsation frequency, $f_0 = 2.559196$ day^{-1} with a $\sigma_{f_0} = 1.485. 10^{-6}$ day^{-1}, and its harmonics up to the 30th order (Figure 3). Figure 5 demonstrates the strong nonlinearity of the fundamental radial mode, showing that the harmonic main-frequency amplitude ratio follows a strong exponential variation along the harmonic order. However, the high orders fails to comply with this scenario: a standstill appears at the 12th order. The same phenomenon was detected and interpreted in the CoRoT RR Lyrae stars (Chadid et al. 2010; Benkő et al. 2016).

3.2. Gravity Modes and Harmonics

After prewhitening the spectrum with the main pulsation frequency and its harmonics, a dominant peak is detected at the frequency $g_0 = 2.001301$ day^{-1} with a $\sigma_{g_0} = 1.523. 10^{-5}$ day^{-1}, and its harmonics at 5th order. Significant frequencies,
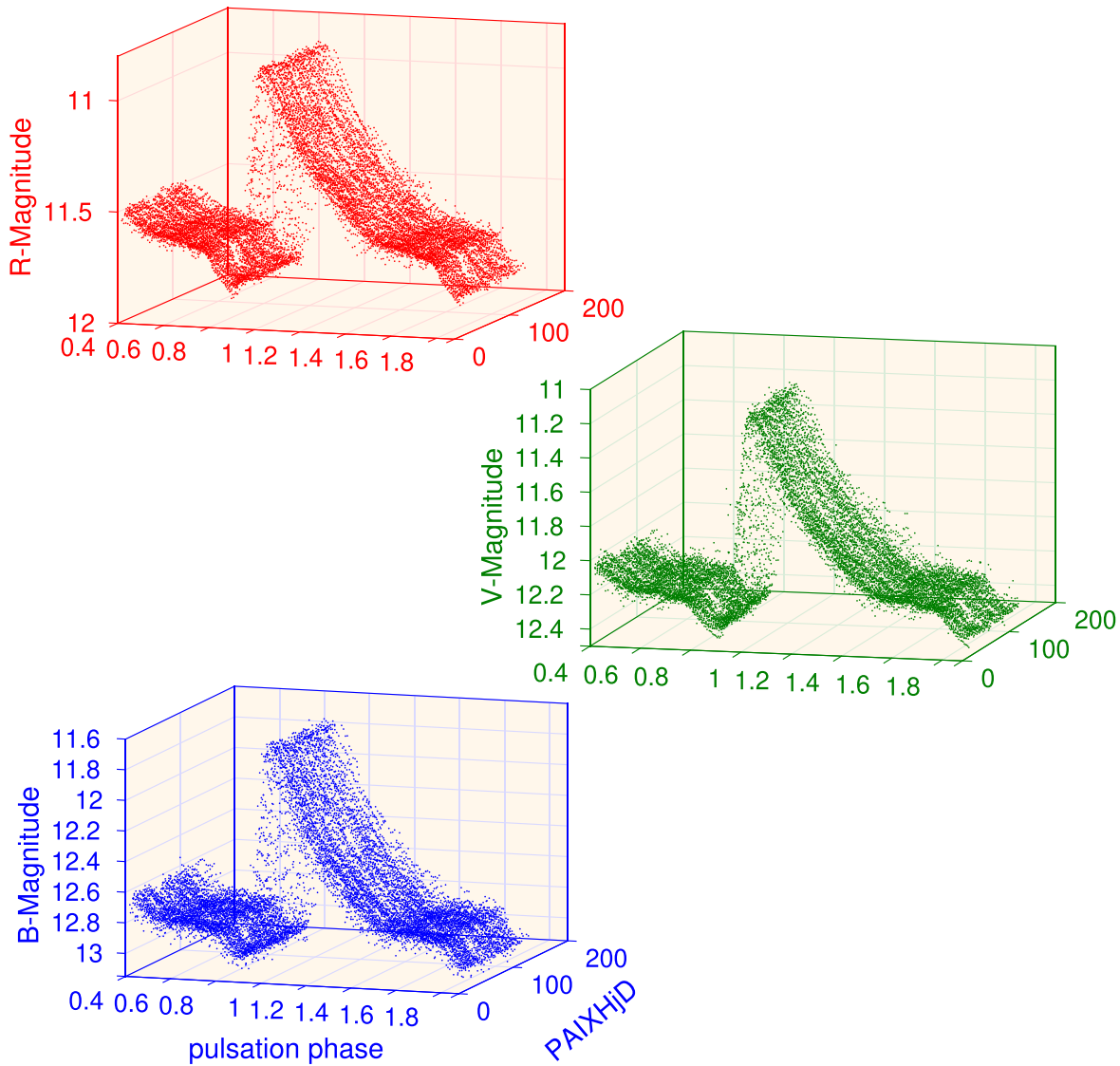
Figure 1. Three-dimensional observed PAIX light curve of RR Lyrae star HH Puppis folded with the pulsation period (0.390 day), during the observing run of 2011's polar wintertime. Axes refer to pulsation phase, magnitude, and PAIX Heliocentric Julian Day.

$g_3 = 0.835433$ day$^{-1} \pm 0.00002$, $g_2 = 1.150662$ day$^{-1} \pm 0.00002$, $g_4 = 1.233302$ day$^{-1} \pm 0.00002$, and $g_1 = 1.498787$ day$^{-1} \pm 0.00002$, are detected with harmonics at 2nd order (Figure 4). A detailed analysis reveals a complex structure in the frequency domain around the dominant peaks g_0, g_3, g_2, g_4, and g_1. All these frequencies are interacting with the fundamental frequency f_0. Such combination terms between g_0, g_3, g_2, g_4, g_1 and the fundamental radial frequency f_0 exclude the possibility that g_0, g_3, g_2, g_4, g_1 are actually related to a background contact system, measured with HH Puppis in the PAIX window. The list of detected frequencies is given in Table 3. It is a great challenge to find an answer to the origin of g_0, g_3, g_2, g_4, and g_1. The rotation period, tidal effects, and higher-order radial overtones pressure modes can be excluded as an explanation for the occurrence of these frequencies. The frequencies seem to be too short to be the rotation period of the RR ab star HH Puppis (Preston et al. 2019) or be connected to the orbital period. We could hardly explain the combination terms in this framework. The frequencies are lower than the fundamental radial frequency f_0; higher-order radial overtones radial pressure modes can be easily excluded, as well.

The most striking features are that these frequencies are lower and show frequency ratios to the fundamental frequency f_0 of $g_0/f_0 = 0.78$, with a period ratio f_0/g_0 to the main pulsation period P_0 of 1.28; $g_1/f_0 = 0.58$, with a period ratio f_0/g_1 to the main pulsation period P_0 of 1.72; $g_2/f_0 = 0.45$, with a period ratio f_0/g_2 to the main pulsation period P_0 of 2.22; $g_3/f_0 = 0.33$, with a period ratio f_0/g_3 to the main pulsation period P_0 of 3.03; and $g_4/f_0 = 2.22$, with a period ratio f_0/g_4 to the main pulsation period P_0 of 2.08. We explain g_0, g_3, g_2, g_1, and g_4 as gravity modes. Such gravity modes must be nonradial modes, since for radial oscillations the perturbation in the gravitational field is eliminated analytically (Christensen-Dalsgaard 1998).

Table 1 gives the amplitude ratio between the fundamental main frequency and the gravity modes. This table shows that the nonradial gravity mode, g_0, is the dominant pulsation mode after the main fundamental frequency, f_0, and is characterized by a nonlinear behavior as shown by the harmonic gravity-mode amplitude ratio evolution (Figure 5) and the pronounced nonsinusoidal shape of its light curve in Figure 2. The additional frequencies $1/2 \, g_0 = 1.0006743$ day^{-1}, $3/2 \, g_0 = 3.001673$

Table 1
Summary of the Relevant Period Ratios to Main Pulsation Period and Amplitude Ratios of HH Pup

Frequency	g_4	g_3	g_2	g_1	g_0	f_0	f_1	f_3	f_2	h_0
Spectral significance	210.90	270.45	215.78	110.92	350.12	2910.88	180.97	140.63	198.50	135.37
Period ratio	2.08	3.03	2.22	1.72	1.28	1	0.56	0.43	0.61	0.84
Amplitude ratio	72.72	58.31	67.96	125.41	49.32	1	92.60	101.26	81.46	101,66

day^{-1}, $5/2\,g_0 = 5.003268$ day^{-1}, and $7/2\,g_0 = 7.004667$ day^{-1} might be the half-integer frequencies of the nonradial gravity mode g_0. The third half-integer frequency $3/2\,g_0$ is the dominant one. Following this hypothesis, the presence of half-integer frequencies would be a clear sign of a period-doubling bifurcation in gravity mode in HH Puppis. Such phenomenon has already been reported by Buchler & Moskalik (1992) in the fundamental radial pressure mode in Population II Cepheids.

3.3. High-order Overtones Pressure Modes

A detailed analysis reveals that the power spectrum has a complex structure in the frequency domain around f_0 and g_0. After prewhitening of the dominant radial frequency, f_0, and the gravity frequencies and their harmonics, we see many additional peaks in the Fourier spectrum (Figure 3). We clearly detect three independent frequencies: (1) $f_2 = 4.211334$ day$^{-1} \pm 0.00002$, with a period ratio f_0/f_2 to the main pulsation period P_0 of 0.61, and an amplitude ratio A_0/A_2 of 81.46; (2) $f_1 = 4.604627$ day$^{-1} \pm 0.00002$, with a period ratio f_0/f_1 to the main pulsation period P_0 of 0.56, and an amplitude ratio A_0/A_1 of 92.60; (3) $f_3 = 5.921856$ day$^{-1} \pm 0.00002$, with a period ratio f_0/f_3 to the main pulsation period P_0 of 0.43, and an amplitude ratio A_0/A_3 of 101.26. Table 1 gives the relevant values of period, frequency, and amplitude ratios. The frequencies f_2, f_3, and f_1 consist of linear combinations of the fundamental radial mode, gravity modes and their harmonics. The origin of the frequencies f_2, f_3 and f_1 is a great challenge. Judging from the period ratio alone, the period ratios f_0/f_2 and f_0/f_3 of 0.61 and 0.43, respectively, are very close to those of the second and third overtones to the fundamental radial mode. Thus, frequencies f_2 and f_3 are likely related to the second and third radial overtone pressure mode, respectively. In fact, the 0.61 period ratio matches the second-overtone period ratio perfectly in Figure A2 of Nemec et al. (2011). Furthermore, such period ratio has been observed in multiple RR ab stars, giving more credence to the notion that the second overtone may become excited with low amplitude in these stars (Molnár et al. 2017). The 0.43 ratio borderline matches the calculated Optical Gravitational Lensing Experiment (OGLE) third-overtone RR Lyrae 0.45–0.48 range in Figure 7 of Smolec et al. (2016). On the other hand, the period ratio of f_1 to the fundamental radial mode is 0.56. Such an unexpected period ratio of 0.56 might be interpreted as a nonradial mode. The additional frequencies $3/2\,f_3 = 8.88293$ day^{-1} might be the third half-integer frequency of the third radial overtone pressure mode. A new group of double periodic stars, in OGLE Galactic bulge photometry, was detected with period ratios 0.68–0.72. The nature of such additional periodicity still remains unknown (Prudil et al. 2017; Smolec et al. 2016). On the other hand, Netzel & Smolec (2019) and Netzel et al. (2015) detected an additional period, longer than the expected period of the radial first overtone mode in OGLE RR c stars, and concluded that it

is not obvious to connect such additional periodicity to a gravity or mixed mode.

3.4. Blazhko Modulations and Nonradial Pressure Modes

Besides the nonradial pressure mode $f_1 = 4.604627$ day^{-1}, we detect the independent frequency $h_0 = 3.043605$ day$^{-1} \pm 0.00002$. This frequency appears at a period ratio f_0/h_0 to the main pulsation period P_0 0.84 with harmonics up to the 6th order (Figure 3). Figure 5 demonstrates that the h_0 harmonic-frequency amplitude ratio follows a low quasi-exponential decrease. The frequency h_0 consists of linear combinations of the fundamental, multiovertones, and gravity modes and their harmonics (Table 3). We interpret h_0 as a nonradial pressure mode in HH Puppis.

From a purely mathematical point of view, when a periodic signal is modulated both in the amplitude and phase, the Fourier spectrum shows an infinite series of side-peak structures with asymmetric amplitudes between the higher and lower frequency sides. The frequency analysis of HH Puppis in this study shows a modulation multiple structure $mf_0 \pm kf_B$. As shown in Figure 3 a triplet structure $f_0 \pm f_B$ is clearly detected, showing a Blazhko frequency $f_B = 0.031039$ day^{-1} (Blazhko period of 32.22 days). We detect also a quintuplet structure $f_0 \pm 2f_B$ and septuplet structure $f_0 \pm 3f_B$ and their harmonics (Table 3). The multiplet side peaks (left and right) show an asymmetry. Such asymmetry is caused by the amplitude difference between the right and left side peaks. The right-side peaks have a higher amplitude than the corresponding left-side ones. We do not directly detect f_B as an independent frequency in the frequency spectrum. This explains the weak behavior of the Blazhko effect in HH Puppis shown in Figure 2. Finally, in defiance of an extensive literature claiming that HH Puppis is a non-Blazhko star, we put into evidence that HH Puppis is a bona-fide Blazhko star. Figure 6 gives an illustration of the complex frequency structure of different radial and nonradial pressure and gravity-oscillating modes in HH Puppis.

Finally, Figure 3(c) shows the residual spectrum prewhitening of all the frequencies that we identified. To check our frequency solution, we ran the program package SigSpec, which calculates the spectral significance defined by Reegen (2007) for each frequency of the spectrum. We use the sig = 5 value as an overall criterion. The spectral significance value is given in Table 1.

4. Fundamental Parameters

A good synthesis of the available formulae to compute the physical characteristics of RR Lyrae stars can be found in Nemec et al. (2011). We use here Sandage's (2004) methods to estimate metal abundances:

1. Using the period–amplitude relation

$$[\mathrm{Fe}/\mathrm{H}] = -1.453 A_0 - 7.990 \log P - 2.145, \qquad (2)$$
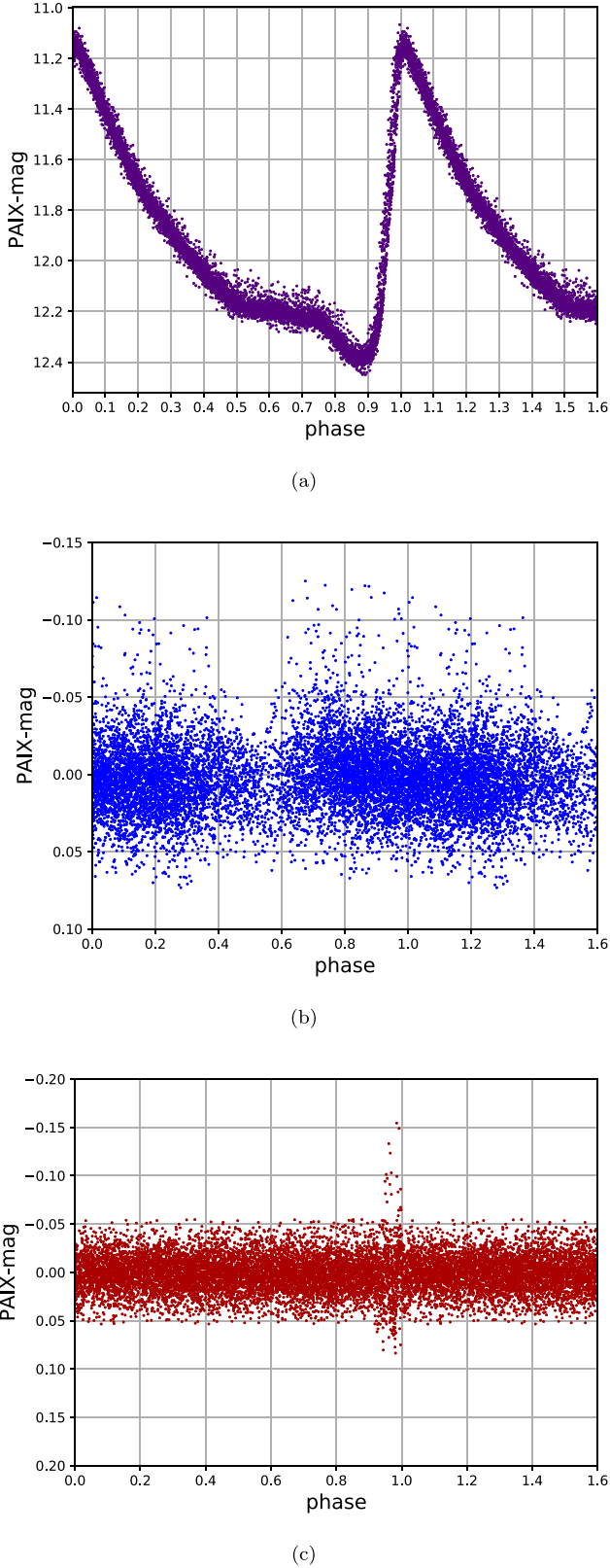
(a)

(b)

(c)

Figure 2. Folded PAIX light curve of RR Lyrae star HH Puppis. From the upper to lower panels: (a) folded with the fundamental period, P_0; (b) folded with the fundamental period P_0 after removal of P_0 and harmonics, its multiovertones pressure modes, their combination frequencies, Blazhko modulations, and the additional nonradial pressure mode frequency and harmonics; (c) folded with P_0 after removal of all detected frequencies shown in Table 3.

we obtain a [Fe/H] value of -0.53 ± 0.043 dex. The coefficients have uncertainties of ± 0.027 and ± 0.091, respectively (from Sandage 2004).

2. The period–rise time relation

$$[\text{Fe/H}] = 6.33\text{RT} - 9.11 \log P - 4.60, \quad (3)$$

where RT is the rise time, giving a [Fe/H] value of -0.25 dex.

from the period–amplitude relation and the period–rise time relation, respectively.

3. The period–phase relation

$$[\text{Fe/H}] = 1.411\Phi_{31} - 7.012 \log P - 6.025, \quad (4)$$

where Φ_{31} is the Fourier phase parameters for a cosine version which differ by π radians with the one derived from a sine version: $\phi_{31}^c = \phi_{31}^s - 3.14159$ (using s and c superscripts for phase parameter computed with, respectively, sine and cosine series). The Φ_{31} and the $\log P$ coefficients have, respectively, uncertainties of ± 0.014 and ± 0.071 (from Sandage 2004). We derive a [Fe/H] value for a cosine version of 4.51 ± 0.078 dex.

As discussed by Nemec et al. (2011), systematic discrepancies are seen between each of these three methods. We adopt the results from the period–amplitude method with a [Fe/H] value of -0.53 ± 0.043 dex. The [Fe/H] value derived from the period–phase relation is very high. Such issue is due to the very high number of frequency components, which induces an overfitting and thus alters the phase values. Moreover, we state that our fundamental parameters study is generated, as described in Section 2, by use of the V-filter passband (λ_{eff} = 540 nm and $\Delta\lambda$ = 100 nm), which is much narrower than the Kepler spectral passband (400–850 nm) from which Nemec's results have been inferred. High-resolution echelle spectra from our previous HH Puppis studies give a [Fe/H] spectroscopic value of -0.95 dex (Preston et al. 2019) and -0.69 dex (Chadid et al. 2017). A recent spectrocopic estimation of the HH Puppis [Fe/H] shows a value of -0.73 dex (Crestani et al. 2021). Such high-spectroscopic studies compare very favorably the estimated -0.53 dex period–amplitude method with the other methods.

We calculate the dereddened mean $B - V$ color from Walker et al. (2001):

$$(B - V) = 0.189 \log P - 0.313A_1 + 0.293A_3 + 0.460, \quad (5)$$

$$\log g = 2.473 - 1.226 \log P, \quad (6)$$

$$\log T_{\text{eff}} = 3.8840 - 0.3219(B - V) + 0.0167 \log g + 0.0070[\text{Fe/H}]. \quad (7)$$

We infer a $B - V$ value of 0.303 mag, a mean surface gravity of 2.971, which is higher than the high spectroscopic values listed in Chadid et al. (2017), and an effective temperature value of 6790 K.

Following Caputo et al.'s (2000) stellar evolution models, we calculated the absolute magnitude, Pulsation luminosity, and mass:

$$M_V = 0.18[\text{Fe/H}] + 1.05, \quad (8)$$

giving a M_V value of 0.95 ± 0.01 (the uncertainties are from Nemec et al. 2011):

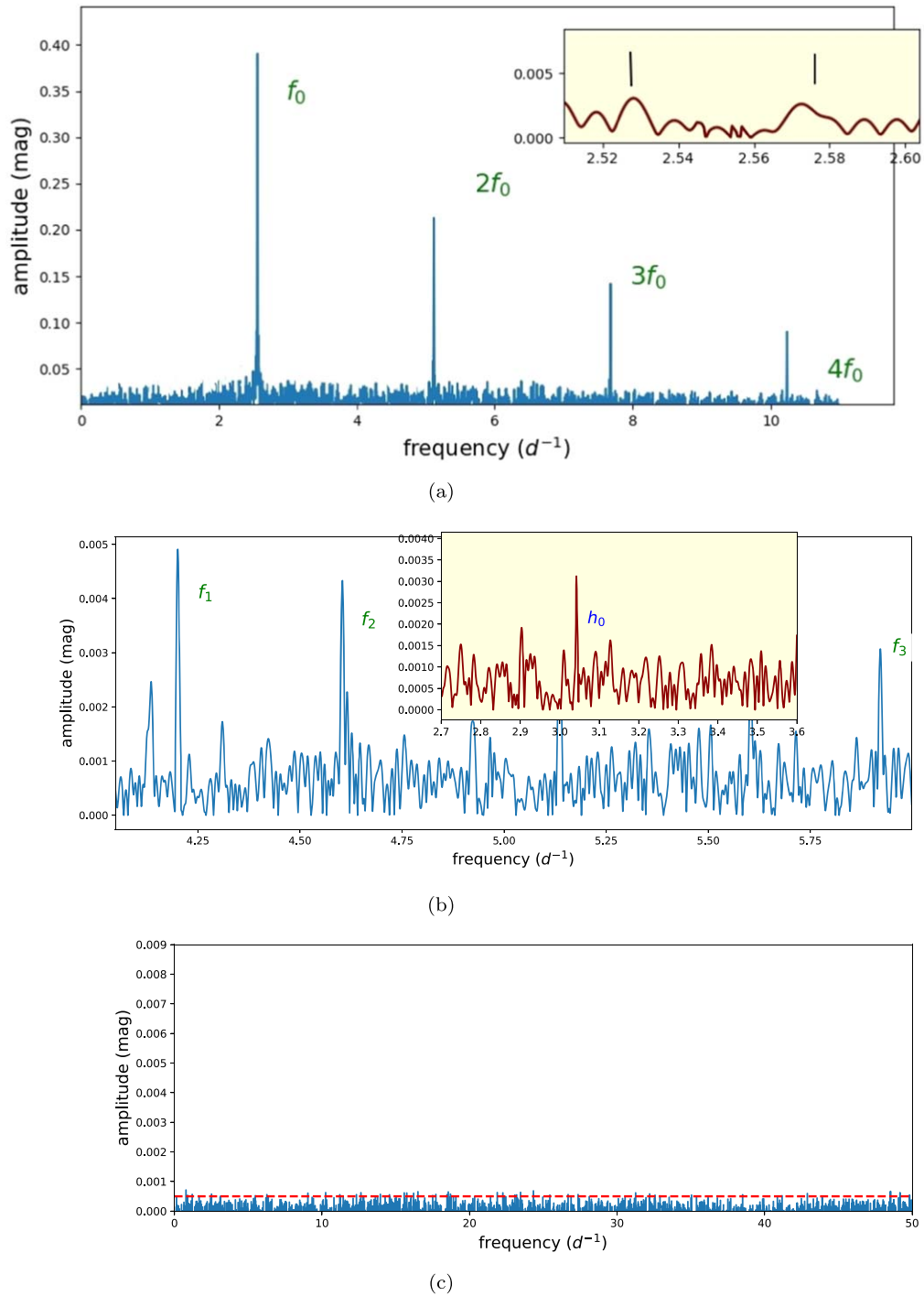$$\log L = 1.538 - 0.110[\text{Fe/H}], \quad (9)$$

(a)

(b)

(c)

Figure 3. (a) The amplitude spectrum of the PAIX light curve of RR Lyrae star HH Puppis; the inset panel shows the modulated peaks $f_0 \pm f_B$. (b) After prewhitening the fundamental radial frequency, the nonradial gravity modes, their harmonics and their linear combination terms; the inset panel shows the nonradial frequency h_0. (c) The residuals after prewhitening with all frequencies in Table 3. The dashed curve shows the noise level that corresponds to the level of the weakest amplitude in the data.

showing a L value of 39.5:

$$\log M = -0.283 - 0.066[Fe/H], \qquad (10)$$

inferring a mass value of $0.57\,M_\odot$.

Table 2 summarizes the main results of HH Puppis's fundamental parameters.

5. Shock Waves and Dynamics

As described by Chadid et al. (2014), shock waves induce a high distortion in the RR Lyrae light curve (Figure 1). Multiple bumps were observed by Chadid et al. (2014) and interpreted as a multishock structure in the RR Lyrae atmosphere. More recently, Prudil et al. (2017) have determined the centers and
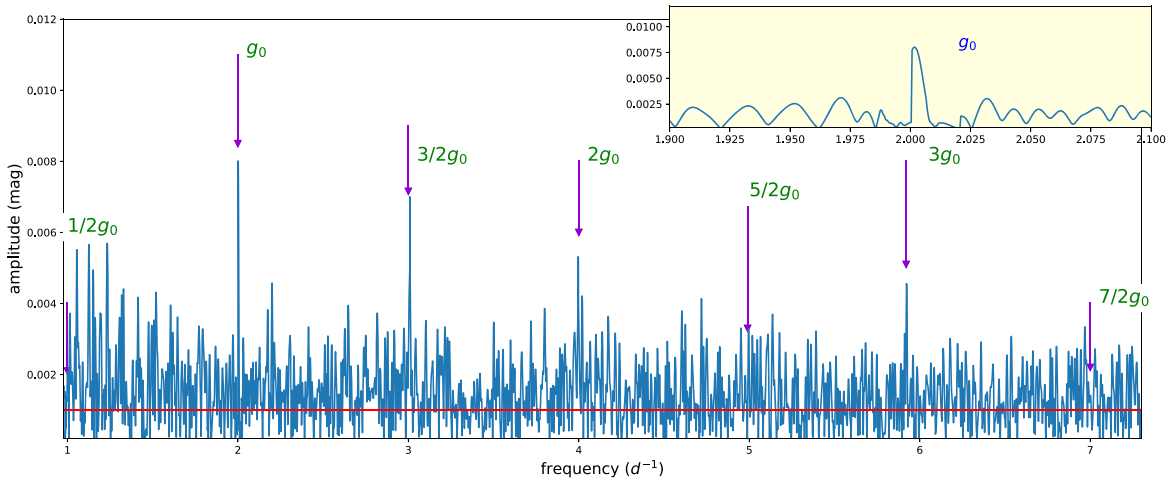
Figure 4. (a) The amplitude spectrum of the PAIX light curve of RR Lyrae star HH Puppis after prewhitening the fundamental radial frequency, f_0, and its harmonics; the inset panel shows the nonradial gra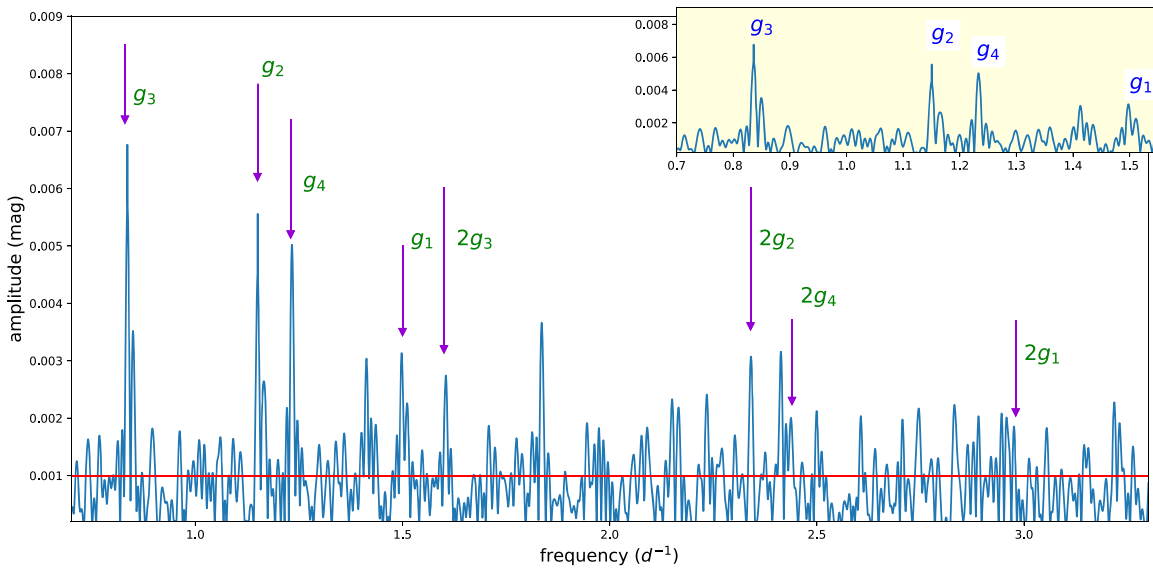vity frequency, g_0. (b) After prewhitening the fundamental radial frequency, its harmonics, the nonradial gravity frequency g_0 and its harmonics; the inset panel shows the nonradial gravity frequencies g_1, g_2, g_3, and g_4.

strengths of main and early shock features in the phased fundamental-mode RR Lyrae light curves. Figure 2 shows the residual light curve after prewhitening with the whole detected frequencies in Table 3, in an attempt to remove all excited oscillating modes from the data set. The most striking feature of the residual light curve is the intense variation that appears around phase 0.95 in a narrow 8% phase interval of the pulsation cycle. Such variation induced by a strong shock wave, named Sh_{H+He} by Chadid et al. (2014), was created by the κ and γ mechanisms traversing the photosphere of HH Puppis during the rise time of the light curve. Such a strong shock wave is at the origin of the hump observed just before the light-curve maximum during the successive pulsation cycle (Chadid & Chapellier 2006; Chadid & Preston 2013). A similar residual scatter had been already observed at the light-curve maxima of the Blazhko star S Arae occurring in a phase interval of 10% of the pulsation period. DR Andromeda, RR Lyr, and RR Gem show a similar residual scatter, as well,
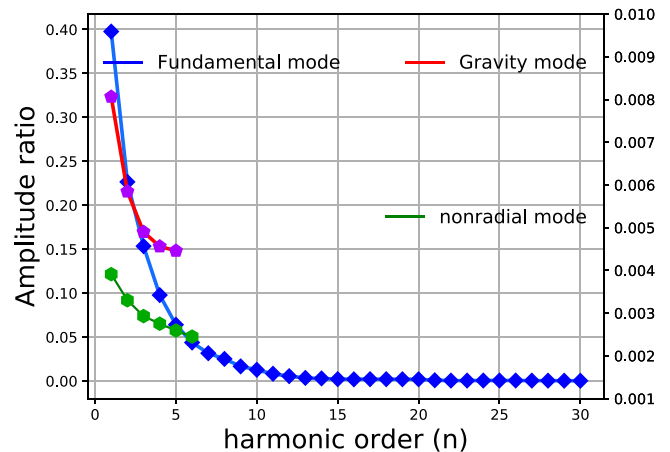

Figure 5. Amplitude ratios of the harmonic components of the fundamental radial pulsation, the gravity mode, and the nonradial pressure pulsation.
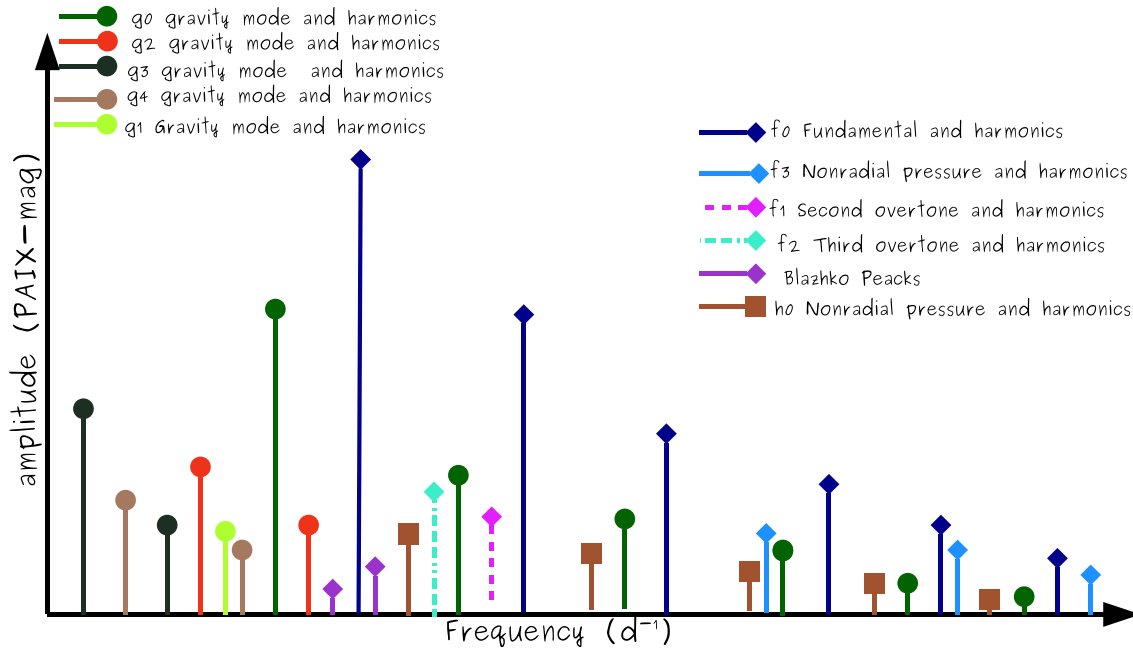
Figure 6. Illustration of the complex frequency structure of multiple radial and nonradial pressure and gravity modes, their harmonics and subharmonics, and modulation peaks in HH Puppis.

Table 2
Observational Characteristics of HH Puppis

[Fe/H] (dex)	$(B-V)$ (mag)	$\log g$	T_{eff} (K)	M_V	L	M $(M_\odot)$
-0.53 ± 0.043	0.303	2.971	6790	0.95 ± 0.01	39.5	0.57

occurring in a phase interval of 20% of the pulsation cycle. This means that the variation in the main shock strength is higher in HH Puppis than in those stars.

6. Excitation Mechanism of Gravity Waves in RR Lyrae Stars

Our results show that HH Puppis is a metal-rich Blazhko RR ab star. According to Chadid et al.'s classification (2017), HH Puppis is a hypersonic-regime RR ab star showing a large gravity acceleration;[1] its dynamical atmosphere shows a high dynamical acceleration and a great Sh_{H+He} main shock Mach number. The most striking finding in this study is that HH Puppis has an even richer Fourier spectrum, and undergoes at the same time p and g modes. Such simultaneity of gravity and pressure modes results from the coupling of pressure waves that probe the atmosphere and gravity waves that probe the radiative core, giving a direct access to the core of HH Puppis.

The detection of any g-mode signals in the Sun, let alone in solar-like stars, is still a highly contentious issue today. The major argument consists in the difficulty in proving a possible mechanism for g-mode excitation. The pressure modes propagate at high frequencies through the convective zone up to the surface, while gravity modes are trapped at low

frequencies in the radiative interior. In the convection zone, hence outside the radiative region, the gravity waves are evanescent. G modes have been predicted and detected in solar-type stars. They have been a treasure trove for red-giant asteroseismology, as described by Bedding et al. (2011) and Beck et al. (2011). Both studies pointed out that the g modes are nonradial modes.

In RR Lyrae stars, Van Hoolst et al. (1998) and Dziembowski (2016) theoretically predicted that there is no gravity wave cavity for radial modes and that the evanescent between the g- and p-mode cavities is narrower for $l = 2$, 3, and 4, where strong mixing can be expected. Moreover, the driving rates drop dramatically for $l = 1$ modes below the fundamental-mode frequency (Dziembowski 2016). On the other hand, internal gravity waves are an efficient transport mechanism in the stellar radiative zone (Schatzman 1993). Strong downward plumes induce a substantial distance extension into the adjacent stable zones, then the internal gravity waves are randomly generated (Hurlburt et al. 1986). The downward plumes are born in the upper-envelope convective layers, are accelerated by the buoyant force, and finally end their life in the overshoot region after transferring a large amount of their stored kinetic energy to the stably stratified medium, resulting in an internal gravity wave field. This convective penetration strongly depends on the value of the local Péclet number (Zahn 1991; Dintrans et al. 2005). The depth of the penetration in the stably stratified zone is a crucial parameter in the excitation mechanism: the stronger the Péclet number, the thinner the penetration and lower the gravity wave excitation. When the Péclet number is larger the plume is rapidly stopped by the buoyancy breaking. In the opposite case, the Péclet number being smaller implies that the buoyancy breaking rapidly disappears, leading to a large penetration and higher excitation of the internal gravity waves. We assume that the convective envelope in RR Lyrae stars is large enough to create a small local Péclet number, which induces an adequate penetration power that is sufficiently able to excite the very small g-mode amplitudes, as detected in this study. Accordingly, we may hypothesize that the

---

[1] The term dynamical acceleration is associated with the primary acceleration induced by the Sh_{H+He} primary shock. The term gravity acceleration is associated with the secondary acceleration and the term gravitational acceleration is $\log g$.

Table 3
Relevant Frequencies and Their Fourier Amplitudes, Phases, and Their Identification

Frequency (day^{-1})	Amplitude (mag)	Phase (cycles)	ID
A—Main fundamental pressure mode frequency and harmonics			
2.559196	0.397679	0.501680	f_0
5.118375	0.226581	0.162268	$2f_0$
7.677543	0.153467	0.870234	$3f_0$
10.236743	0.097789	0.728544	$4f_0$
12.795857	0.064069	0.215091	$5f_0$
15.355083	0.043846	0.007674	$6f_0$
17.914130	0.031658	0.866588	$7f_0$
20.473334	0.025181	0.917582	$8f_0$
23.032741	0.016695	0.235621	$9f_0$
25.592196	0.012829	0.884852	$10f_0$
28.151083	0.008318	0.248028	$11f_0$
30.710335	0.005599	0.555862	$12f_0$
33.268002	0.003571	0.469407	$13f_0$
35.828500	0.003000	0.480355	$14f_0$
38.387956	0.002193	0.851552	$15f_0$
40.947905	0.001961	0.981247	$16f_0$
43.506891	0.002156	0.241041	$17f_0$
46.066245	0.002121	0.348781	$18f_0$
48.625231	0.002034	0.753122	$19f_0$
51.181787	0.002055	0.396982	$20f_0$
52.995878	0.000902	0.441381	$21f_0$
55.994399	0.000510	0.385783	$22f_0$
57.995152	0.005274	0.387343	$23f_0$
60.995253	0.000573	0.722048	$24f_0$
62.997290	0.000596	0.750047	$25f_0$
66.004626	0.000603	0.958771	$26f_0$
68.996565	0.000486	0.808693	$27f_0$
70.994377	0.000435	0.447202	$28f_0$
73.988838	0.000372	0.336705	$29f_0$
76.001869	0.000324	0.556226	$30f_0$
B—Second and third overtone mode frequencies, harmonics and subharmonics			
4.211334	0.004882	0.622764	f_2
5.921856	0.003927	0.200287	f_3
11.840311	0.004298	0.968200	$2f_3$
8.88293	0.003954	0.675503	$3/2f_3$
17.766750	0.003612	0.738022	$3f_3$
C—Gravity-mode frequencies, harmonics and subharmonics			
2.001301	0.008064	0.937279	g_0
4.003510	0.005846	0.954913	$2g_0$
6.005067	0.004900	0.190098	$3g_0$
8.006805	0.004562	0.541087	$4g_0$
10.005108	0.004463	0.784127	$5g_0$
1.0006743	0.001978	0.124666	$1/2g_0$
3.001893	0.007024	0.295939	$3/2g_0$
5.003268	0.002896	0.200007	$5/2g_0$
7.004667	0.002469	0.055471	$7/2g_0$
0.835433	0.006820	0.971325	g_3
1.670510	0.003702	0.381325	$2g_3$
1.150662	0.005852	0.624346	g_2
2.301243	0.003946	0.041390	$2g_2$
1.233302	0.005469	0.562601	g_4
2.466715	0.003412	0.222470	$2g_4$
1.498787	0.003171	0.834126	g_1
2.997876	0.001578	0.018760	$2g_1$
E—Blazhko multiplet frequencies			
2.528157	0.003964	0.967529	$f_0 - f_B$

Table 3
(Continued)

Frequency (day^{-1})	Amplitude (mag)	Phase (cycles)	ID
2.590235	0.005161	0.367529	$f_0 + f_B$
2.497206	0.003196	0.529648	$f_0 - 2f_B$
2.621230	0.004440	0.368648	$f_0 + 2f_B$
2.652499	0.003167	0.255279	$f_0 + 3f_B$
2.466099	0.002887	0.535975	$f_0 - 3f_B$
F—Nonradial pressure modes and harmonics			
3.043605	0.003912	0.125482	h_0
6.087216	0.003302	0.009045	$2h_0$
9.130828	0.002931	0.179416	$3h_0$
12.174814	0.002753	0.419028	$4h_0$
15.219031	0.002550	0.865765	$5h_0$
18.261935	0.002421	0.578192	$6h_0$
4.604627	0.004287	0.905535	f_1
G—Linear combinations			
12.238282	0.004053	0.205536	$4f_0 + g_0$
12.76466	0.002540	0.438686	$5f_0 - f_B$
10.267802	0.003196	0.333569	$4f_0 + f_B$
5.561218	0.004942	0.649476	$f_0 + 3/2g_0$
28.181595	0.002912	0.530506	$11f_0 + f_B$
4.560559	0.005007	0.496673	$f_0 + g_0$
6.559175	0.002883	0.250258	$f_0 + 2g_0$
7.1637440	0.003445	0.265586	$f_1 + f_0$
4.529445	0.002558	0.481783	$f_0 - fB + g_0$
1.599963	0.003358	0.978659	$2g_4 - g_3 - f_B$
7.962294	0.004340	0.982464	$2g_4 + f_0 + 3/2g_0 - 2f_B$
10.68000	0.004693	0.596918	$3f_0 + 3/2g_0$
3.792523	0.003350	0.877481	$f_0 + g_4$
0.397909	0.005559	0.459725	$g_4 - g_3$
6.794516	0.003678	0.066399	$g_4 + f_0 + 3/2g_0$
0.257877	0.004355	0.927123	$f_0 - 2g_2$
0.907092	0.004258	0.666979	$2f_0 - f_2$
8.910838	0.003131	0.897412	$3f_0 + g_4$
0.514026	0.003989	0.402010	$f_1 - 2f_0$
2.836750	0.002325	0.456325	$g_0 + g_3$
1.652510	0.003702	0.381325	$f_2 - f_0$
9.723002	0.002660	0.639489	$f_1 + 2f_0$
4.057497	0.002214	0.602944	$f_0 + g_1$
1.325947	0.003478	0.235078	$f_0 - g4$
2.014383	0.004472	0.964364	$f_1 - f_0 - f_B$
3.072640	0.002314	0.546870	$3f_0 - f_1$
11.039989	0.003333	0.921603	$2f_0 + f_3$
14.402945	0.003289	0.751847	$2f_3 + f_0$
9.222667	0.003901	0.017743	$2f_3 - f_0 - 2fB$
5.045954	0.002640	0.943928	$f_2 + g_3$
6.212879	0.004764	0.663111	$f_2 + g_0$
2.209971	0.004708	0.442860	$f_2 - g_0$
3.920347	0.004708	0.719098	$f_3 - g_0$
8.213945	0.002876	0.711630	$f_2 + 2g_0$
0.208515	0.008043	0.226481	$f_2 - 2g_0$
4.180270	0.003220	0.196335	$f_2 - f_B$
5.890860	0.002701	0.929047	$f_3 - f_B$
21.218494	0.006013	0.515658	$5f_0 + 2f_2$
3.105684	0.002758	0.955653	$h_0 + 2f_B$
4.276853	0.002923	0.465204	$h_0 + g_4$
7.254879	0.003575	0.078563	$h_0 + f_2$
1.167822	0.005257	0.918952	$f_2 - h_0$
7.648301	0.003989	0.866471	$h_0 + f_1$
1.755697	0.004325	0.650188	$f_3 - 3f_0$
11.562553	0.003138	0.264277	$5f_0 - g_4$
7.584791	0.003024	0.112463	$2f_0 + 2g_4$

Frequency (day^{-1})	Amplitude (mag)	Phase (cycles)	ID
16.588501	0.002601	0.618216	$6f_0 + g_4$
10.133190	0.002539	0.215918	$f_2 + f_3$
4.285721	0.002827	0.887962	$4f_0 - f_3$
3.977686	0.002974	0.889681	$3f_0 - 3g_4$
14.031970	0.002273	0.884726	$5f_0 + g_4$

(This table is available in its entirety in machine-readable form.)

excitation of internal gravity waves in RR Lyrae stars is possible by the penetration of convective plumes into the adjacent stably stratified radiative zone. It is worth highlighting that the treatment of convective contributions on stellar stability in RR Lyrae stars is a serious problem and has been debated for decades. As recently suggested by Stellingwerf (2013), the convective envelopes of RR Lyrae stars are deeper. de Lira (2010) found that shocks encountering the density inhomogeneities characteristic of convective envelopes generate turbulent velocities that dissipate shocks; thus, he attributed such shock-energy dissipation to larger convective envelopes in RR Lyrae stars. More recently, Chadid et al. (2017) detected that the photospheric radii and the radius variations of RR Lyrae stars are larger, and are a direct consequence of the greater thicknesses of their compression zones. In that way, they concluded that RR Lyrae stars have larger convective envelopes. However, the understanding of the process associated with convection in RR Lyrae stars makes our hypothesis on the mechanism of gravity wave excitation a challenging endeavor. Conclusively, the RR Lyrae pulsation is excited by several distinct mechanisms: the κ–γ mechanisms and the radiation-modulated excitation mechanism that induce pressure waves, and the penetrative convection mechanism that induces gravity waves. We hypothesize that the key process in the Blazhko mechanism is the gravity waves, which play a trigger role. The pressure waves, induced by the κ–γ mechanisms, are perturbed by the gravity waves induced by the convection mechanism, leading to cyclic modulations, the so-called Blazhko effect. Additional theoretical efforts will be addressed in our theoretical subsequent paper focused on a numerical modeling toward a better understanding of these issues.

7. Summary

We investigate unprecedented time-series ground-based observations, by use of PAIX in the highest plateau of Antarctica over one polar night, and an extensive frequency analysis, leading us to some important conclusions. The first and by far the most important one is the detection of gravity modes in RR Lyrae stars. The power spectrum of HH Puppis shows a complex frequency structure: in particular, dominant peaks occur at low frequencies, showing nonradial gravity modes. These lower frequencies and harmonics linearly interact with the dominant fundamental radial pressure mode and its second and third overtone pressure modes. Half-integer frequencies of g modes are detected, likewise side-peak structures, demonstrating that HH Puppis is a bona-fide Blazhko star.

We interpret the excitation mechanism of internal gravity waves in RR Lyrae stars by penetrative convection. We demonstrate that RR Lyrae stars undergo several distinct pressure oscillating excitation driving mechanisms: (1) the κ and γ mechanisms occur in hydrogen and helium ionization zones, inducing an outward radiative shock, Sh_{H+He}; (2) the radiation-modulated excitation mechanism occurs in a zone of the radiation flux gradient, which is the bottom and the top of the convective zone, inducing an outward radiative shock, Sh_{RME}; and (3) the gravity-oscillating excitation mechanism, convection mechanism occurs just below the photosphere.

Finally, we hypothesize that the Blazhko effect is a nonlinear gravito-hydrodynamic interplay between the gravitation waves, which play the trigger role, intimately connected to the convective zone right below the photosphere, and the pressure waves provided by variations of the opacity in the H and He ionization zones, κ and γ driving mechanisms.

ORCID iDs

Merieme Chadid ● https://orcid.org/0000-0001-9441-7875

References

Alcock, C., Alves, D. R., Becker, A., et al. 2003, ApJ, 598, 597
Auvergne, M., Bodin, P., Boisnard, L., et al. 2009, A&A, 506, 411
Bailey, S. I. 1902, AnHar, 38, 1
Beck, P. G., Bedding, T. R., Mosser, B., et al. 2011, Sci, 332, 205
Bedding, T. R., Mosser, B., Huber, D., et al. 2011, Natur, 471, 608
Benkő, J. M., Plachy, E., Szabó, R., Molnár, L., & Kolláth, Z. 2014, ApJS, 213, 31
Benkő, J. M., Szabó, R., Derekas, A., & Sódor, Á. 2016, MNRAS, 463, 1769
Bessell, M. S. 2005, ARA&A, 43, 293
Blažko, S. 1907, AN, 175, 325
Buchler, J. R., & Kolláth, Z. 2011, ApJ, 731, 24
Buchler, J. R., & Moskalik, P. 1992, ApJ, 391, 736
Caputo, F., Castellani, V., Marconi, M., & Ripepi, V. 2000, MNRAS, 316, 819
Chadid, M. 2012, A&A, 540, A68
Chadid, M., Benkő, J. M., Szabó, R., et al. 2010, A&A, 510, A39
Chadid, M., & Chapellier, E. 2006, A&A, 456, 305
Chadid, M., Kolenberg, K., Aerts, C., & Gillet, D. 1999, A&A, 352, 201
Chadid, M., & Preston, G. W. 2013, MNRAS, 434, 552
Chadid, M., Sneden, C., & Preston, G. W. 2017, ApJ, 835, 187
Chadid, M., & Vernin, J. 2019, MNRAS, 484, 3620
Chadid, M., Vernin, J., Abe, L., et al. 2016, Proc. SPIE, 9908, 99080T
Chadid, M., Vernin, J., & Gillet, D. 2008, A&A, 491, 537
Chadid, M., Vernin, J., Jumper, G. Y., Liu, L. Y., & Trinquet, H. 2018, Proc. SPIE, 10702, 107020N
Chadid, M., Vernin, J., Preston, G., et al. 2014, AJ, 148, 88
Chadid, M., Wade, G. A., Shorlin, S. L. S., & Landstreet, J. D. 2004, A&A, 413, 1087
Christensen-Dalsgaard, J. 1998, Lecture Notes on Stellar Oscillations (Aarhus Universitet: Institut for Fysik og Astronomi), https://books.google.fr/books?id=FD55cgAACAAJ
Crestani, J., Fabrizio, M., Braga, V. F., et al. 2021, ApJ, 908, 20
de Lira, C. H. R. 2010, PhyS, T142, 014022
Dintrans, B., Brandenburg, A., Nordlund, Å., & Stein, R. F. 2005, A&A, 438, 365
Dziembowski, W. A. 2016, CoKon, 105, 23
Dziembowski, W. A., & Mizerski, T. 2004, AcA, 54, 363
Gilliland, R. L., Jenkins, J. M., Borucki, W. J., et al. 2010, ApJL, 713, L160
Hurlburt, N. E., Toomre, J., & Massaguer, J. M. 1986, ApJ, 311, 563

Koch, D. G., Borucki, W. J., Basri, G., et al. 2010, ApJL, 713, L79
Lenz, P., & Breger, M. 2005, CoAst, 146, 53
Molnár, L., Bódi, A., Pál, A., et al. 2022, ApJS, 258, 8
Molnár, L., Plachy, E., Klagyivik, P., et al. 2017, European Physical Journal Web of Conferences, 160, 04008
Molnár, L., Szabó, R., Moskalik, P. A., et al. 2015, MNRAS, 452, 4283
Nemec, J. M., Smolec, R., Benkő, J. M., et al. 2011, MNRAS, 417, 1022
Netzel, H., & Smolec, R. 2019, MNRAS, 487, 5584
Netzel, H., Smolec, R., & Dziembowski, W. 2015, MNRAS, 451, L25
Nowakowski, R. M., & Dziembowski, W. A. 2001, AcA, 51, 5
Preston, G. W., Sneden, C., Chadid, M., Thompson, I. B., & Shectman, S. A. 2019, AJ, 157, 153
Prudil, Z., Smolec, R., Skarka, M., & Netzel, H. 2017, MNRAS, 465, 4074
Reegen, P. 2007, A&A, 467, 1353
Sandage, A. 2004, AJ, 128, 858

Schatzman, E. 1993, A&A, 279, 431
Shibahashi, H., & Takata, M. 1995, in ASP Conf. Ser. 83, IAU Coll. 155: Astrophysical Applications of Stellar Pulsation, ed. R. S. Stobie & P. A. Whitelock (San Francisco, CA: ASP), 42
Smolec, R., Prudil, Z., Skarka, M., & Bakowska, K. 2016, MNRAS, 461, 2934
Soszyński, I., Udalski, A., Wrona, M., et al. 2019, AcA, 69, 321
Stellingwerf, R. F. 2013, arXiv:1310.0535
Stothers, R. B. 2010, PASP, 122, 536
Van Hoolst, T., Dziembowski, W. A., & Kawaler, S. D. 1998, in ASP Conf. Ser. 135, A Half Century of Stellar Pulsation Interpretation, ed. P. A. Bradley & J. A. Guzik (San Francisco, CA: ASP), 232
Walker, A. R., Raimondo, G., Di Carlo, E., et al. 2001, ApJL, 560, L139
Zahn, J. P. 1991, A&A, 252, 179
Zalian, C., Chadid, M., & Stellingwerf, R. F. 2014, MNRAS, 440, 68